Thermoelectric Response Driven by Spin-State Transition in $La_{1-x}Ce_xCoO_3$ Perovskites

Yang Wang,[†,‡] Yu Sui,[*,†,§] Xianjie Wang,[†] Wenhui Su,[†] Wenwu Cao,[†,#] and Xiaoyang Liu[||]

Center for Condensed Matter Science and Technology (CCMST), Department of Physics, Harbin Institute of Technology, Harbin 150001, People's Republic of China, Division of Physics and Applied Physics, School of Physical and Mathematical Sciences, Nanyang Technological University, 21 Nanyang Link, 637371, Singapore, International Center for Materials Physics, Academia Sinica, Shenyang 110015, People's Republic of China, Materials Research Institute, The Pennsylvania State University, University Park, Pennsylvania 16802, and State Key Laboratory of Inorganic Synthesis and Preparative Chemistry, College of Chemistry, Jilin University, 2699 Qianjin Street, Changchun 130012, People's Republic of China

ABSTRACT An unusual thermoelectric response was observed in n-type perovskite oxide $La_{1-x}Ce_xCoO_3$. Combining transport and magnetic measurements, we found that the thermoelectric response is driven by the spin-state transition of Co^{3+}. This transition destroys the spin blockade effect and induces an abrupt decrease of resistivity as well as an insulator−metal transition. In contrast to the resistivity change, changes in thermopower and thermal conductivity are moderate. Consequently, a peak of figure of the merit ZT is present in a narrow temperature range. The room-temperature $ZT \approx 0.018$ of $La_{0.94}Ce_{0.06}CoO_3$ is comparable to that of p-type Na_xCoO_2. These observations can be helpful for the search and design of new thermoelectric materials.

KEYWORDS: thermoelectric • electron-doping • spin-state transition • spin blockade • configuration entropy

INTRODUCTION

Environmentally friendly thermoelectric (TE) materials have been widely studied for a long time because they hold great promise for clean energy generation. Good TE materials require a large thermopower S, a low resistivity ρ, and a small thermal conductivity κ in order to achieve a high figure of merit $Z = S^2/\rho\kappa$. Usually, ZT larger than one is necessary for practical applications, where T is the absolute temperature. Unfortunately, good natural TE materials are rare. To date, only a few state-of-the-art alloys exhibit $ZT > 1$ (1). Recently, TE oxides have attracted a renewed interest because of their many advantages compared with traditional TE alloys (2). Among various metal oxides, n-type manganites, titanates, doped In_2O_3 and ZnO, and p-type cobaltites exhibit large TE response, and thus several all-oxide TE power generators have been fabricated by using these oxides (2−11). For instance, single-crystalline $(Ca_2CoO_3)_{0.7}CoO_2$ exhibits $ZT \approx 0.87$ at 973 K (11); Nb-doped $SrTiO_3$ epitaxial thin films show ZT∼0.37 at 1000 K (4); ZT of doped In_2O_3 ceramics can reach ∼0.3 around 1000 K (8, 9); ZT values of Al, Ga dually doped ZnO can reach 0.47 at 1000 K and 0.65 at 1247 K (10), which appear to be the highest ZT so far for bulk n-type oxides. These high ZT values obtained in oxides suggest that the application of all-oxide TE devices may be on the horizon.

Among these TE metal oxides, cobalt oxides exhibits some interesting TE behaviors due to their complex spin/orbital configurations which are the probable origin of high TE performance (12). In addition to layered cobaltites (2, 11), perovskite-type $LaCoO_3$ systems are also considered as potential TE oxide materials. Several reports have pointed out that the substitution of divalent Sr^{2+} or Ca^{2+} for La^{3+} (hole-doping) can noticeably decrease ρ while S remains a relatively high level (5, 13−15). In contrast, the investigations on TE properties of electron-doped $LaCoO_3$ (e.g., tetravalent Ce^{4+} doped $LaCoO_3$) are still scarce. Electron-type $La_{1-x}Ce_xCoO_3$ has been widely investigated as catalyst for exhaust gas depollution (16). The magnetic properties of $La_{1-x}Ce_xCoO_3$ have also been studied both experimentally and theoretically (17−19). Hebert et al. recently found that $La_{0.99}Ce_{0.01}CoO_3$ exhibits a high negative S value, but ρ is also quite large (20). Nevertheless, limited by the solubility of Ce dopant, the preparation of single-phase bulk material $La_{1-x}Ce_xCoO_3$ with $x > 0.03$ is difficult (18). So the TE properties of $La_{1-x}Ce_xCoO_3$ with higher Ce content remain unexplored up to date.

In this study, we adopt a cold high-pressure method to synthesize $La_{1-x}Ce_xCoO_3$ ceramics in a wider doping range and investigate their TE properties. A TE response is found in a narrow temperature range in these compounds. The transport and magnetic results reveal that the observed TE response is driven by the spin-state transition of Co^{3+}.

* Corresponding author. E-mail: suiyu@hit.edu.cn.
Received for review March 19, 2010 and accepted July 9, 2010
† Harbin Institute of Technology.
‡ Nanyang Technological University.
§ Academia Sinica.
# The Pennsylvania State University.
|| Jilin University.
DOI: 10.1021/am100243e

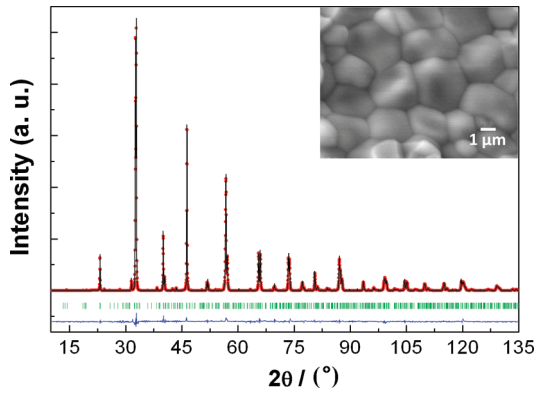

FIGURE 1. Room-temperature XRD pattern and the Rietveld refinement result for $La_{0.94}Ce_{0.06}CoO_3$. The experimental data are shown as dots; the global fitting profile and the difference curve are shown as solid lines; the calculated reflection positions are indicated by stick marks. The inset shows the SEM image of the cross-section for cold-pressed $La_{0.94}Ce_{0.06}CoO_3$.

EXPERIMENTAL SECTION

Polycrystalline $La_{1-x}Ce_xCoO_3$ ($0 \leq x \leq 0.06$) samples were prepared by a standard solid-state reaction followed by a cold high-pressure process. A mixture of high-purity La_2O_3, CeO_2, and Co_3O_4 powders in stoichiometric quantities was ground and pressed into disk-shaped pellets. Then, they were sintered at 1473 K in air for 24 h with intermediate grindings. To obtain dense ceramic samples, the products were repeatedly ground and cold pressed into pellets under a high pressure of 3 GPa, and then sintered at 1473 K in air for 24 h. The detailed process of this cold high-pressure synthesis is shown in Supporting Information.

The powder X-ray diffraction (XRD) data at room temperature were collected by using the XRD diffractometer (Advanced D8) with Cu Kα ($\lambda = 0.15406$ nm) radiation. The data were collected from 10° up to 135° in 2θ with 0.02° step and a counting time of 30 s per step. Rietveld refinement was performed to determine the structural parameters by using the profile analysis program Fullprof. The XRD data and the refinement results confirmed the formation of single-phase compounds. We also fabricated several specimens with Ce content $x > 0.06$, but the XRD data revealed CeO_2 and Co-oxides impurities in those specimens. Hence, the solubility of Ce in our cold high-pressure synthesized $La_{1-x}Ce_xCoO_3$ samples is ~0.06. Iodometic titration indicated the oxygen content fell in the range of 3.01−3.02. Details of the iodometric titration had been described in ref 21. Microstructure and energy-dispersive spectrum (EDS) measurements were performed using a JEOL JSM-6700F scanning electron microscope (SEM).

Temperature dependences of the resistivity, thermopower, thermal conductivity, Hall coefficient, and magnetic susceptibility were measured from 20 to 350 K by using the physical property measurement system (Quantum Design PPMS). Resistivity and thermopower at elevated temperatures were measured by ULVAC-RIKO ZEM-3. High-temperature thermal conductivity was determined by the thermal diffusivity (Netzsch LFA-427), specific heat capacity (Netzsch DSC-404), and density. These results revealed that the $x = 0.06$ sample exhibited the optimal TE response, so we will mainly discuss the results of $La_{0.94}Ce_{0.06}CoO_3$.

RESULTS AND DISCUSSION

As shown in Figure 1, the XRD patterns show that $La_{1-x}Ce_xCoO_3$ ($x \leq 0.06$) samples are single-phase with rhombohedral $R\bar{3}c$ crystalline structure. The structural parameters, determined by Rietveld refinement, are listed in Table 1. The lattice parameter a and β decrease systematically with increasing Ce content. These results indicate that Ce doping does not change the crystalline structure of this system, but induces a reduction in the unit-cell volume as well as a weakening of the rhombohedral distortion. The EDS results confirmed the gradual increase in Ce content in our $La_{1-x}Ce_xCoO_3$ samples from $x = 0.01$ to 0.06 (see the Supporting Information). The $\rho-T$ curves for $La_{1-x}Ce_xCoO_3$, as shown in the Supporting Information, indicate that the resistivity ρ decreases monotonously with Ce content until $x = 0.06$. This could be attributed to the increase in electrons induced by Ce doping. However, when the doping level exceeds 0.06, ρ begins to increase slightly. This phenomenon may result from the insulating impurities. It also confirmed that the Ce solubility is around 0.06 in our cold-pressed samples, which is consistent with the XRD results.

Table 1. Lattice Parameters, Atomic Positions, Isotropic Thermal Factor B_{iso}, and Fitting Factors (R_{wp}, R_B, and R_F) for the $La_{1-x}Ce_xCoO_3$ Samples

	$x = 0$	$x = 0.01$	$x = 0.03$	$x = 0.06$
a (Å)	5.3812(6)	5.3808(5)	5.3790(6)	5.3779(5)
β (deg)	60.7021(8)	60.6924(8)	60.6210(10)	60.5286(8)
B_{iso}(La) (Å^2)	0.23(3)	0.23(3)	0.24(3)	0.23(3)
B_{iso}(Co) (Å^2)	0.27(3)	0.27(4)	0.28(4)	0.28(4)
x_O	0.21018(20)	0.21052(18)	0.21177(22)	0.21295(21)
y_O	0.28982(25)	0.28948(22)	0.28823(24)	0.28705(27)
B_{iso}(O) (Å^2)	0.76(4)	0.79(5)	0.78(4)	0.81(5)
R_{wp} (%)	8.36	8.52	8.79	9.12
R_B (%)	4.55	4.71	4.69	4.78
R_F (%)	3.61	3.63	3.68	3.76

Fuchs et al. synthesized $La_{1-x}Ce_xCoO_3$ ceramics by a sol−gel method and found that the preparation of single-phase bulk material of $La_{1-x}Ce_xCoO_3$ with $x > 0.03$ was very difficult (18). However, their prepared $La_{1-x}Ce_xCoO_3$ ($0.1 \leq x \leq 0.4$) epitaxial thin films are all single-phase (18). This indicates that the Ce solubility is noticeably enhanced in the strained thin films. Considering the similarities of substrate-induced pressure and applied high pressure, we speculate that the Ce solubility should be also enhanced in the high-pressure synthesized samples. From the XRD and resistivity results as discussed above, it is clear that the Ce solubility has been enhanced to 0.06 in our high-pressed $La_{1-x}Ce_xCoO_3$ specimens. From the SEM image (see the inset of Figure 1), these high-pressure synthesized samples are quite dense, without any obvious pores. The density of the samples is in the range of ~7.10−7.15 g/cm^3, very close to the theoretical density (7.29 g/cm^3). The typical grain size is ~3 μm.

Figure 2 shows the temperature dependences of the resistivity ρ, thermopower S, thermal conductivity κ, and ZT of $La_{0.94}Ce_{0.06}CoO_3$. The huge ρ below 50 K is meaningless to a TE material, so we only present the transport parameters and ZT values above 50 K. Below ~250 K, the $\rho-T$ curve of $La_{0.94}Ce_{0.06}CoO_3$ is insulating-like (i.e., $d\rho/dT < 0$), similar with that of pure $LaCoO_3$. S is negative in the whole measured temperature range, indicating the nature of electron carrier (n-type). A remarkable features of this material

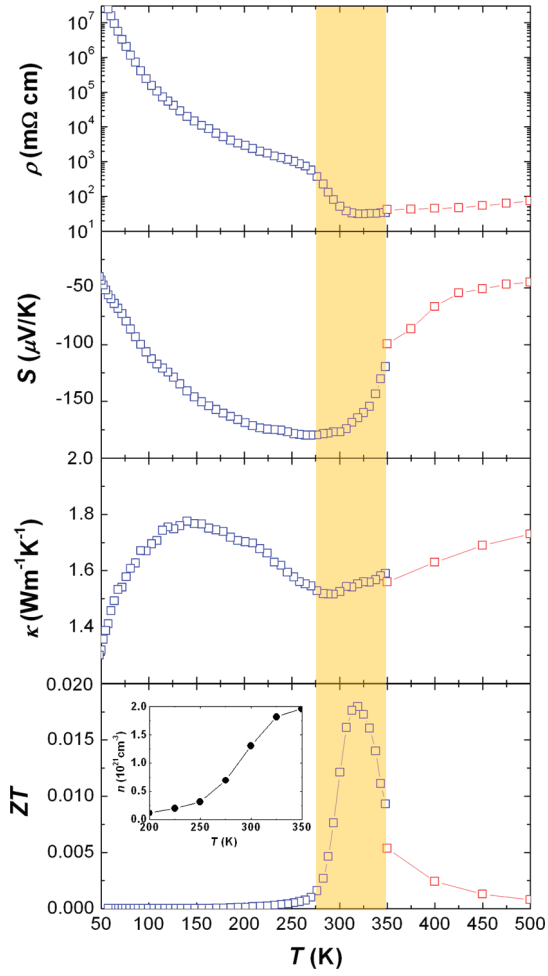

FIGURE 2. Temperature dependences of resistivity ρ, thermopower S, thermal conductivity κ, and figure of merit ZT of $La_{0.94}Ce_{0.06}CoO_3$. Because of the different measure equipments, the low-temperature data (blue squares) and high-temperature data (red squares) cannot change smoothly. The shadow area indicates the temperature range for noticeable TE response. The inset in $ZT-T$ plot gives the temperature dependence of carrier concentration n.

is that ρ exhibits a step-shaped drop in a narrow temperature range (as sketched by the shadow area in Figure 2) near room temperature, after which a metallic-like temperature dependence (i.e., $d\rho/dT > 0$) is observed. In the same temperature range, the absolute value of S shows a decrease, whereas the low-temperature broad peak in the $\kappa-T$ curve is suppressed, followed by a $d\kappa/dT > 0$ behavior. As a result, the ZT exhibits a steep peak and reaches 0.018 at room temperature. This room-temperature ZT value is close to the value observed in the layered Na_xCoO_2 ($ZT \approx 0.03$) (22), but is much smaller than that of the perovskite-type hole-doped $LaCoO_3$ ($ZT \approx 0.1$) (15).

The rapid decrease in ρ in this temperature range can be attributed to the considerable increase in carrier concentration n, evidenced by the Hall measurements (see the inset of Figure 2). To probe the source of these interesting variations of transport parameters, the magnetic susceptibility χ under 1000 Oe field was measured. The $\chi^{-1}-T$ curve clearly indicates that the system undergoes a magnetic transition around 250 K that is just the onset temperature of the steep variations in the transport parameters (see Figure 3). Since

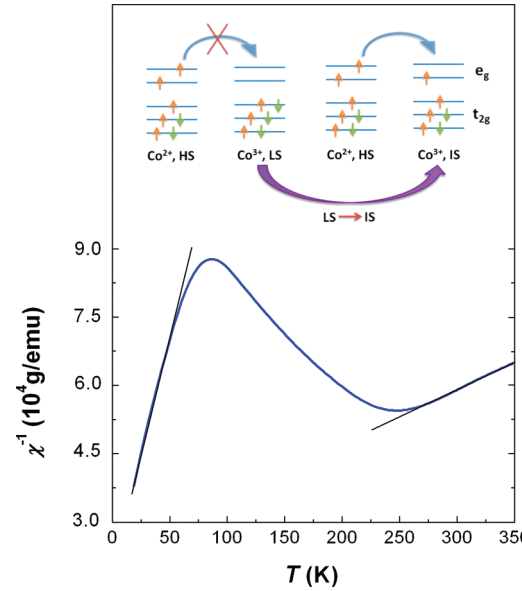

FIGURE 3. Inverse susceptibility χ^{-1} as a function of T for $La_{0.94}Ce_{0.06}CoO_3$. The solid lines in $\chi^{-1}-T$ are the linear fittings. The inset presents a sketch for the e_g electron hopping processes between HS Co^{2+} and LS Co^{3+}, and between HS Co^{2+} and IS Co^{3+}.

the substitution of Ce^{4+} for La^{3+} brings Co^{2+} ions to Co^{3+} matrix, and Co^{2+} is always a high-spin (HS, $t_{2g}^5e_g^2$) ion (23), the change in χ is reminiscent of the spin-state transition of Co^{3+}. (Although Zhang et al. theoretically suggested a LS ground state of Co ions for $x < 0.08$ in $La_{1-x}Ce_xCoO_3$ (19), their conclusion is different from our observations herein and Maignan et al.'s experimental results (23); see the discussions below.) It has been confirmed that nonmagnetic $LaCoO_3$ undergoes a spin-state transition from a low-spin state (LS, t_{2g}^6) to an intermediate-spin state (IS, $t_{2g}^5e_g^1$) at ~100 K, above which $LaCoO_3$ exhibits paramagnetic behavior (24–26). Both carrier and chemical pressure have important effects on the spin-state transition. Divalent Ca^{2+} or Sr^{2+} doping introduces large numbers of hole carriers, which suppresses the nonmagnetic ground state and then stabilizes the IS state, causing the LS-IS transition shifts to lower temperatures (25, 26). Nevertheless, when the carriers introduced by doping are limited, the doping-induced chemical pressure becomes dominant. (Herein although Ce doping introduces electron carriers, the carrier concentration of $La_{1-x}Ce_xCoO_3$ is still very low compared with that of hole-doped $LaCoO_3$, so the chemical pressure plays a key role in the spin-state transition.) Because chemical pressure increases the crystal field splitting energy, the substitution of La by other rare-earth ions with smaller radius stabilizes the LS state to higher temperatures (27–29). Accordingly, considering that the radius of Ce^{4+} is much smaller than that of La^{3+}, it is reasonable to assume that Ce^{4+} doping will increase the LS–IS transition temperature.

To confirm this assumption, we performed an analysis of the effective magnetic moments by fitting the χ^{-1}-T curve using the Curie–Weiss law below 80 K and above 275 K, respectively. Below 80 K, the fitting gives the effective moment of $\mu_{eff} \approx 0.62\ \mu_B$ per Co ion, where μ_B is the Bohr magneton. Assuming a single-electron picture where $\mu_{eff} =$

$g_e \times \sqrt{S(S+1)}$, with the electron g factor $g_e = 2$, this μ_{eff} value corresponds to a total spin $S = 0.083$. This spin value implies that ~5.8% Co^{2+} ions are HS, whereas all the 94% Co^{3+} ions are LS, which is well-consistent with our situation. Above 275 K, the fitting gives $\mu_{eff} \approx 2.04\ \mu_B$ and thus $S = 0.67$. Taking into account a two-level spin system of Co^{3+} consisting of LS and IS, this spin value corresponds to 6% Co^{2+} ions in HS, 58% Co^{3+} ions in IS, and 36% Co^{3+} ions in LS. The ratio of IS Co^{3+} and LS Co^{3+} ions is comparable to that observed in $LaCoO_3$ bulks and polycrystalline films around room temperature (30). This result suggests that most Co^{3+} ions are already in the IS state above 275 K.

The spin-state transition scenario is compatible with the electrical and thermal transport behaviors, and can well elucidate the observed unusual TE response at room temperature. Considering the configurations of Co^{2+} (HS) and Co^{3+} (LS and IS) (see the inset of Figure 3), the charge transport depends strongly on the spin state of the background Co^{3+}. In the LS Co^{3+} situation, moving one e_g electron of Co^{2+} to empty e_g orbitals of the LS Co^{3+} is forbidden, because that will simultaneously change the spin states of Co^{2+} and Co^{3+}, and lead to wrong configurations: LS Co^{2+} and IS Co^{3+}. Therefore, the electric conduction process will be strongly suppressed. Accordingly, the charge transport can only be achieved by thermal excitation of electrons in the initially empty conduction band, which thus results in large resistivity, poor carrier concentration, an insulating-like $\rho-T$ behavior. Herein the charge transport scenario is similar to the spin blockade effect as proposed for layered perovskite cobaltites (23). Nevertheless, once the LS → IS transition takes place as temperature rises, the charge transport will be much facilitated. The hopping of e_g electrons between Co^{2+} and IS Co^{3+} is very easy because of the degenerate configurations of HS Co^{2+} and IS Co^{3+}, namely, e_g electrons become delocalized. Consequently, a large number of electron carriers and a high conductivity appear. The obvious increase in e_g electron carriers also widens the e_g bandwidth because of a strong electron interaction. When the e_g band is widened to approach the narrow-band limit of itinerant electrons, the system will show metallic-like $\rho-T$ behavior. That is why the insulator−metal transition occurs and $d\rho/dT > 0$ is observed at elevated temperatures.

On the other hand, the considerable increase in n must cause a rapid reduction of S. However, n is not the unique factor in determining S; S of cobaltites is also strongly dependent on the rich spin/orbital degeneracies of Co ions (12). At high enough temperatures, S of doped cobaltites is expected to be determined by the Heikes formula

$$S = \frac{k_B}{e}\left[\ln\left(\frac{n}{1-n}\right) + \ln\left(\frac{g_2}{g_3}\right)\right] \quad (1)$$

where g_2 and g_3 denote the number of Co^{2+} and Co^{3+} configurations, respectively (12, 13). Although this model assumes a high temperature limit, Koshibae et al. had pointed out that S in cobaltites at room temperature is close to that at the high temperature limit, so this model is appropriate for an approximate evaluation of S near room temperature (12). According to eq 1, one can calculate that the LS → IS transition of Co^{3+} will yield an increment of S (denoted by ΔS) approximately equal to $-144\ \mu V/K$ because of the contribution of configurational entropy. Detailed calculation is presented in the Supporting Information. The calculated ΔS roughly agrees with the observed S value in the LS → IS transition (approximately -160 to $-120\ \mu V/K$). Therefore, although a large number of carriers induced by spin-state transition reduce S, the reduction of S is partially compensated by the contribution of configurational entropy, and hence the decrease in S is not as sharp as that in ρ. Consequently, a peak of TE response is observed in the LS → IS transition temperature range (around room temperature). After the spin-state transition, the entropy does not influence S any more and the compound becomes metallic-like, so that S monotonously decreases with the increase in n. In addition, as $T \to \infty$, S tends to reach a constant value of approximately $-40\ \mu V/K$ that does not depend on carrier concentration. Recently, it has been observed that all the $LaMn_{1-x}Co_xO_3$ ($x > 0.5$) compounds exhibit such an identical S value at high temperature (31).

Furthermore, this spin-state transition scenario is also consistent with the κ-T behavior. Estimated from Wiedemann−Franz law, the phonon thermal conductivity κ_{ph} is dominant in κ, so the variation of κ mainly originates from the change in κ_{ph}. Since Co^{3+} in the IS state is a strongly Jahn−Teller (JT) active ion which can induce larger local distortion, whereas Co^{3+} in the LS state is non-JT active, after the IS → LS transition occurs, the JT distortion vanishes, which will lengthen the average free path of phonons with decreasing temperature, and hereby lead to an evident revival of κ. Accordingly, a broad low-temperature peak in $\kappa-T$ curve appears. As for the positive temperature dependence of κ of $La_{1-x}Ce_xCoO_3$ at high temperature, it is similar to the κ behavior of undoped $LaCoO_3$. It has been reported that the anomalous thermal expansion, lattice disorder, and temperature-induced LS−IS disorder in $LaCoO_3$ cause the glass-like phonon transport behavior at elevated temperatures (13, 32−34). Because κ_{ph} is dominant in κ, similar with the case of $LaCoO_3$, herein $La_{1-x}Ce_xCoO_3$ also exhibits $d\kappa/dT > 0$ above room temperature.

CONCLUSIONS

In summary, the electrical transport, thermal transport, and magnetic measurements reveal a spin-state transition in $La_{1-x}Ce_xCoO_3$. The spin-state transition drives a TE response in a narrow temperature range. The room-temperature ZT of $La_{0.94}Ce_{0.06}CoO_3$ reaches 0.018. Although the present ZT value is still far from application criterion ($ZT > 1$), the occurrence of such a TE behavior in oxide system is exciting. It is well-known that rich spin/orbital configurations and spin-state transitions are widespread in transition-metal oxides, so such TE response driven by spin-state transition may open a new approach to search and design TE oxides.

Acknowledgment. The project was sponsored by the Scientific Research Foundation for the Returned Overseas

Chinese Scholars (State Education Ministry), Natural Scientific Research innovation foundation in Harbin Institute of Technology (HIT. NSRIF.2009056), and National Natural Science Foundation of China (Grant 10804024).

Supporting Information Available: Detailed experimental process of cold high-pressure synthesis, resistivity, and EDS characterization results of $La_{1-x}Ce_xCoO_3$, and the calculation of S based on eq 1 (PDF). This material is available free of charge via the Internet at http://pubs.acs.org.

REFERENCES AND NOTES

(1) Bell, L. E. *Science* **2008**, *321*, 1457–1461.
(2) Ohta, H.; Sugiura, K.; Koumoto, K. *Inorg. Chem.* **2008**, *47*, 8429–8436.
(3) Flahaut, D.; Mihara, T.; Funahashi, R.; Nabeshima, N.; Lee, K.; Ohta, H.; Koumoto, K. *J. Appl. Phys.* **2006**, *100*, 084911.
(4) Ohta, S.; Nomura, T.; Ohta, H.; Hirano, M.; Hosono, H.; Koumoto, K. *Appl. Phys. Lett.* **2005**, *87*, 092108.
(5) Androulakis, J.; Migiakis, P.; Giapintzakis, J. *Appl. Phys. Lett.* **2004**, *84*, 1099–1101.
(6) Matsubara, I.; Funahashi, R.; Takeuchi, T.; Sodeoka, S.; Shimizu, T.; Ueno, K. *Appl. Phys. Lett.* **2001**, *78*, 3627–3629.
(7) Reddy, E. S.; Noudem, J. G.; Hébert, S.; Goupil, C. *J. Phys. D: Appl. Phys.* **2005**, *38*, 3751–3755.
(8) Guilmeau, E.; Bérardan, D.; Simon, Ch.; Maignan, A.; Raveau, B.; Ovono, D. O.; Delorme, F. *J. Appl. Phys.* **2009**, *106*, 053715.
(9) Bérardan, D.; Guilmeau, E.; Maignan, A.; Raveau, B. *J. Appl. Phys.* **2008**, *104*, 064918.
(10) Ohtaki, M.; Araki, K.; Yamamoto, K. *J. Electron. Mater.* **2009**, *38*, 1234–1238.
(11) Masahiro, S.; Funahashi, R. *Appl. Phys. Lett.* **2003**, *82*, 1851–1853.
(12) Koshibae, W.; Tsutsui, K.; Maekawa, S. *Phys. Rev. B* **2000**, *62*, 6869–6872.
(13) Berggold, K.; Kriener, M.; Zobel, C.; Reichl, A.; Reuther, M.; Müller, R.; Freimuth, A.; Lorenz, T. *Phys. Rev. B* **2005**, *72*, 155116.
(14) Iwasaki, K.; Ito, T.; Nagasaki, T.; Arita, Y.; Yoshino, M.; Matsui, T. *J. Solid State Chem.* **2008**, *181*, 3145–3150.
(15) Wang, Y.; Sui, Y.; Ren, P.; Wang, L.; Wang, X. J.; Su, W. H.; Fan, H. J. *Inorg. Chem.* **2010**, *49*, 3216–3223.
(16) Nitadori, T.; Misono, M. *J. Catal.* **1985**, *93*, 459–466.
(17) Zhang, Q. F.; Zhang, W. Y. *Phys. Rev. B* **2003**, *68*, 184403.
(18) Fuchs, D.; Schweiss, P.; Adelmann, P.; Schwarz, T.; Schneider, R. *Phys. Rev. B* **2005**, *72*, 014466.
(19) Zhang, Q. F.; Huang, X. Y.; Zhang, W. Y.; Hu, A. *J. Appl. Phys.* **2004**, *95*, 6822–6824.
(20) Hébert, S.; Flahaut, D.; Martin, C.; Lemonnier, S.; Noudem, J.; Goupil, C.; Maignan, A.; Hejtmanek, J. *Prog. Solid State Chem.* **2007**, *35*, 457–467.
(21) Karppinen, M.; Matvejeff, M.; Salomäki, K.; Yamauchi, H. *J. Mater. Chem.* **2002**, *12*, 1761–1764.
(22) Takahata, K.; Iguchi, Y.; Tanaka, D.; Itoh, T.; Terasaki, I. *Phys. Rev. B* **2000**, *61*, 12551–12555.
(23) Maignan, A.; Caignaert, V.; Raveau, B.; Khomskii, D.; Sawatzky, G. *Phys. Rev. Lett.* **2004**, *93*, 026401.
(24) Kobayashi, Y.; Fujiwara, N.; Murata, S.; Asai, K.; Yasuoka, H. *Phys. Rev. B* **2000**, *62*, 410–414.
(25) Kriener, M.; Zobel, C.; Reichl, A.; Baier, J.; Cwik, M.; Berggold, K.; Kierspel, H.; Zabara, O.; Freimuth, A.; Lorenz, T. *Phys. Rev. B* **2004**, *69*, 094417.
(26) Takami, T.; Zhou, J. S.; Goodenough, J. B.; Ikuta, H. *Phys. Rev. B* **2007**, *76*, 144116.
(27) Demazeau, G.; Pouchard, M.; Hagenmuller, P. *J. Solid State Chem.* **1974**, *9*, 202–209.
(28) Itoh, M.; Mori, M.; Yamaguchi, S.; Tokura, Y. *Physica B* **1999**, *259–261*, 902–903.
(29) Itoh, M.; Hashimoto, J.; Yamaguchi, S.; Tokura, Y. *Physica B* **2000**, *281–282*, 510–511.
(30) Fuchs, D.; Pinta, C.; Schwarz, T.; Schweiss, P.; Nagel, P.; Schuppler, S.; Schneider, R.; Merz, M.; Roth, G.; v. Löhneysen, H. *Phys. Rev. B* **2007**, *75*, 144402.
(31) Autret, C.; Hejtmánek, J.; Knížek, K.; Maryško, M.; Jirák, Z.; Dlouhá, M.; Vratislav, S. *J. Phys.: Condens. Matter* **2005**, *17*, 1601–1616.
(32) Zobel, C.; Kriener, M.; Bruns, D.; Baier, J.; Grüninger, M.; Lorenz, T.; Reutler, P.; Revcolevschi, A. *Phys. Rev. B* **2002**, *66*, 020402R.
(33) Yan, J. Q.; Zhou, J. S.; Goodenough, G. B. *Phys. Rev. B* **2004**, *69*, 134409.
(34) Baier, J.; Jodlauk, S.; Kriener, M.; Reichl, A.; Zobel, C.; Kierspel, H.; Freimuth, A.; Lorenz, T. *Phys. Rev. B* **2005**, *71*, 014443.

AM100243E